metals

MDPI

Article

Design of High Temperature Ti–Al–Cr–V Alloys for Maximum Thermodynamic Stability Using Self-Organizing Maps

Rajesh Jha † and George S. Dulikravich †,*

Department of Mechanical and Materials Engineering, Multidisciplinary Analysis, Inverse Design and Robust Optimization Center (MAIDROC) Laboratory, Florida International University, Miami, FL 33174, USA; rjha001@fiu.edu

* Correspondence: dulikrav@fiu.edu; Tel.: +1-305-348-7016

† These authors contributed equally to this work.

Received: 27 March 2019; Accepted: 8 May 2019; Published: 10 May 2019

Abstract: Data generated for the Ti–Al–Cr–V system of metallic alloys from our previous publication, where the composition of 102 alloys were computationally Pareto optimized with the objective of simultaneously maximizing the Young's modulus and minimizing density for a range of temperatures, was the starting point of the current research, where compositions at different temperatures of these alloys were analyzed for phase stability in order to generate new data for compositions and volume fractions of stable phases at various temperatures. This resulted in a large dataset where a lot of data were still missing as all the phases are not stable at a given temperature for all the compositions. The concept of Self-Organizing Maps (SOM) was then applied to determine correlations between alloy compositions, stabilities of desired phases at various temperatures, associated Young's moduli and densities, and the effect of the composition of phases on these properties. This work should help alloy designers to determine the required chemical composition of a new alloy with reference to the temperature of application of that alloy and see the effect of temperature and composition on stable phases and associated properties of alloys.

Keywords: Self-Organizing Maps; CALPHAD; Thermo-Calc Software 2018B; JMatPro; alloys design

1. Introduction

Titanium alloys possess high strength, fracture toughness, creep strength, excellent resistance to corrosion, and a longer fatigue life at a moderate density when compared to steel and nickel base alloys [1]. As a result, titanium alloys are considered an important structural material in the aerospace industry [1–5]. Currently ~80 % of the global titanium production is consumed by the aerospace industry, and it is used more in military aircraft when compared with commercial aircraft [1]. One of the disadvantages of titanium alloys is their relatively high density (4.5 g/cm^3) when compared to aluminum alloys (2.7 g/cm^3) and carbon–epoxy composites (1.5–2.0 g/cm^3) [1]. Additionally, extraction of titanium is an expensive process [1]. When using it as an aerospace component, it requires a specialized material removal process such as laser-assisted machining to fabricate and shape aircraft components free of machine damage [1,2]. This further adds to the final cost of the titanium alloy parts [1–3].

At room temperature, titanium alloys can have two allotropes: hexagonal close-packed (HCP) known as α-Ti and body centered-cubic (BCC), also known as β-Ti [1–3]. Other alloys such as those based on nickel, aluminum, and magnesium have single crystal structures at room temperature [1]. The allotropy of titanium has been exploited by the researchers resulting in commercial titanium

based alloys produced as α-titanium alloys, near-α-titanium alloys (small amount of β-phase), (α+β)-titanium and near-β-titanium alloys (small amount of α-phase), while β-titanium alloys have not been commercially produced in significant amounts [1,2]. Chemical composition of these two phases is almost identical, but these phases provide different properties to alloys. Specifically, alloys with α-Ti phase possess low-to-medium strength, have good toughness and ductility, are weldable, and possess excellent resistance to creep at high temperatures [1]. On the other hand, alloys with β-Ti phase possess high strength and fatigue resistance, they are heat treatable [1], resistant to creep at intermediate temperatures, and are less ductile than α-Ti alloys [1].

Aluminum is the most common α-stabilizer. Tin has also been used in a few cases [1], whereas Cr, V, Mo, Nb, and Fe are used as β-stabilizers [1]. Titanium has a valency of two, three or four [1]. Any alloying element with lower valency promotes stabilization of α-phase, while elements with valency higher than titanium promote formation of β-phase [1]. Neutral elements such as C, N, Si, and Re are used to improve other desired properties such as tensile strength [1]. Thus, chemical composition and heat treatment significantly affect the stability and amount of desired phase required in the alloy for application at a given temperature [1,2]. It should be pointed out that several undesirable phases can also form during the processing [1,2]. In the context of titanium alloys containing α- and β-phases, the undesirable phases are titanium aluminides, such as Ti3Al (D019), γ-TiAl, and Laves phases. Thus, it is extremely important to understand the correlation between the chemical composition, stability of phases at a given temperature and a range of temperatures, volume fraction of desired phases, concentration of alloying elements in the desired phase, and bulk properties of interest such as Young's modulus and density [1–3].

First commercial use of alloys based on Ti–Al–Cr–V system was as a β alloy [1]. Specifically, Ti-13V-11-Cr-3Al (at. %) was used in the airframe, fuselage frame, wing, longerons, bulkheads, ribs, landing gear, and body skins of Lockheed SR-71 Blackbird supersonic military aircraft [1] where aerodynamic friction and shock waves caused heating of the skin to a temperature of approximately 300 °C [1]. Design process used to develop this alloy was traditional, based on time-consuming classical experimentation, personal experience of the designer, intuition, and empiricism [1–5].

In order to significantly reduce the need for experimentation, reduce the total amount of time spent designing new alloys, and eliminate the subjectivity factor of the designer, we have developed a computational design methodology using multiobjective evolutionary optimization algorithms and response surfaces with periodic experimental verifications [6–11] applicable to arbitrary alloys.

A significant advance in this design methodology applied to Ti–Al–Cr–V system was an attempt [12] to eliminate the need for classical experimentation by combining a commercial software [13] utilizing large experimental databases and thermodynamics of solids in conjunction with a robust commercially available multiobjective optimization software [14]. We are dealing with designing chemistry of alloys for the temperature range of 30 to 1500 °C, while simultaneously optimizing two objectives: Young's modulus and density. Simulations were performed at 30, 200, 400, 600, 800, 1000, 1200, 1300, 1400, and 1500 °C. The result obtained from this was a set of Pareto-optimized candidate alloys for each of the mentioned temperatures. Pareto optimized in the current context means the best trade-off between Young's modulus and density. In the simulations performed through JMatPro (Sente Software, Surrey, UK), stability of equilibrium phases was not checked. Therefore, in this work, we decided to perform calculations under the framework of CALPHAD (calculation of phase diagrams) approach for the Pareto-optimized set of alloys reported in our previous work.

Objective of the current work is to present a further refinement in this alloys design methodology by calculating the amounts and effects of various phases and their stability at different temperatures. For this purpose, an initially Pareto-optimized set of Ti–Al–Cr–V alloys [12] will be enlarged and studied for its physical metallurgy using framework of CALPHAD [15] approach. Thereafter, a study of the entire dataset will be presented to draw correlations between composition, amount (volume fraction) of stable phases at these temperatures, composition (concentration) of alloying elements in these phases, and macroscopic properties such as Young's modulus and density. This alloy design approach will also

help the experimentalists to screen alloys prior to manufacture (including designing heat treatment protocols) by avoiding compositions for which detrimental phases are stable for a composition at a particular temperature.

Stages for designing heat treatment for achieving desired microstructure that will be helpful for achieving desired properties are as follows.

1. Estimate the stability of the desired phases, which is helpful for achieving the desired properties. In this work, we have worked on this part by studying stability of α and β-phases in titanium alloys for a range of compositions and temperatures. Additionally, we have mentioned the formation of undesired phases in the current case, titanium aluminides and Laves phases, for the same temperature and composition range. Thus, a reader can focus on that composition and temperature range prior to designing heat treatment protocol.
2. After determining stability of a phase, it is important to create time–temperature–transformation (TTT) and continuous cooling transformation (CCT) diagrams to study the evolution of the desired phases. Thus, in step 1, the designer should deal with thermodynamics, while in step 2 the focus should be the kinetics of phase transformation.

From steps 1 and 2, an experimentalist has information about the thermodynamics and kinetics of phase transformation for a set of compositions and temperatures from the phase stability calculations and the TTT and CCT diagrams. Then, the experimentalist can design heat treatment protocol that will be helpful in precipitating these phases in desired size ranges, which will define the microstructure and will help in achieving desired macroscopic properties. Grain size and volume fraction of desired phases can be found in the literature.

2. Materials and Methods

In the current work, the original dataset of Pareto-optimized chemical compositions of Ti–Al–Cr–V alloys [12] was further utilized by generating new data for each of the compositions and temperature with another software, Thermo-Calc Software 2018B (Thermo-Calc Software, Stockholm, Sweden) [15], via its TCTI2 thermodynamic database. This new data includes volume fraction of stable phases and concentrations of alloying elements in these phases. Thereafter, a versatile optimization software package modeFRONTIER 4.5 (ESTECO, Trieste, Italy) [16] was applied via the principle of Self-organizing Maps (SOM) [17–23] on this enlarged dataset to draw meaningful conclusions, which proved to be helpful in understanding the correlations between composition, temperature, stable phases, phase compositions, and Young's modulus of elasticity and density of the alloy.

In these computational studies, concentrations of Al were allowed to vary from 0 to 50 wt. %, while Cr and V varied between 0 and 15 wt. % [12]. In α-titanium alloys, aluminum addition is above 9–10 wt. %. In our dataset, most of the alloys had aluminum concentration above 10 wt. %. However, we have two β-stabilizers: Cr and V. Thus, some β-phase will also form. Since aluminum is an α-stabilizer and, in the current study, is present in large amounts when compared to β-stabilizers, Cr, and V, we are dealing with (α + β) titanium alloy system [1–3].

Figure 1 shows the phase diagram of one of the candidate alloys from our dataset (Ti88.34-Al11.15-Cr0.4-V0.11 in wt. %. with Cr fixed at 0.4 wt. % and V fixed at 0.11 wt. %.) where aluminum concentration was allowed to vary, while titanium adds up to the balance. In Figure 1, it can be observed that, apart from HCP_A3 (α) and BCC_B2 (β), there exist several other phases such as titanium aluminides, like TI3AL_D019, TIAL_L10, and C15_LAVES. Even BCC_B2 (β) exists in two forms—ordered and disordered phase—on the phase diagram. We have stated the notations that we observed from Thermo-Calc Software [15]. In Thermo-Calc, while plotting the figures, if we chose "ordering", we get it displayed on the phase diagram. During equilibrium calculations, we observed B2 phase in two forms: BCC_B2 and BCC_B2#2. Thus, we used these notations so that readers can easily follow the phases that were mentioned from the Thermo-Calc Software manual.

There also exists titanium aluminide (Ti_3Al) phase as ALTI3_D019 (α_2), which forms if the aluminum concentration is more than 9% [1,3]. However, Ti_3Al precipitates are brittle and reduce alloy's fracture strength and ductility [1–3]. Titanium aluminides are also used in the aerospace industry as entirely Ti_3Al (α_2)- and γ-TiAl-ordered L10 structure (TIAL_L10) compounds, due to their high-temperature strength and comparatively lower density. Efforts have been made to improve upon ductility and fracture toughness along with the manufacturing cost [1–3].

In this work, further discussion of these phases will be avoided as we are dealing with (α + β) titanium alloy system and titanium aluminide phases are not desired in this system. Thus, we performed equilibrium calculations and estimated the amount of stable phases for 102 alloys at temperatures (30–1500 °C) for which Young's modulus and density have been reported [12]. Thereafter, we analyzed the CALPHAD [15] predictions and found that for several compositions, properties are different, while the amount (volume fraction) of phase is the same. Therefore, we further calculated the concentration of alloying elements in each of the equilibrium phases to better understand the current system.

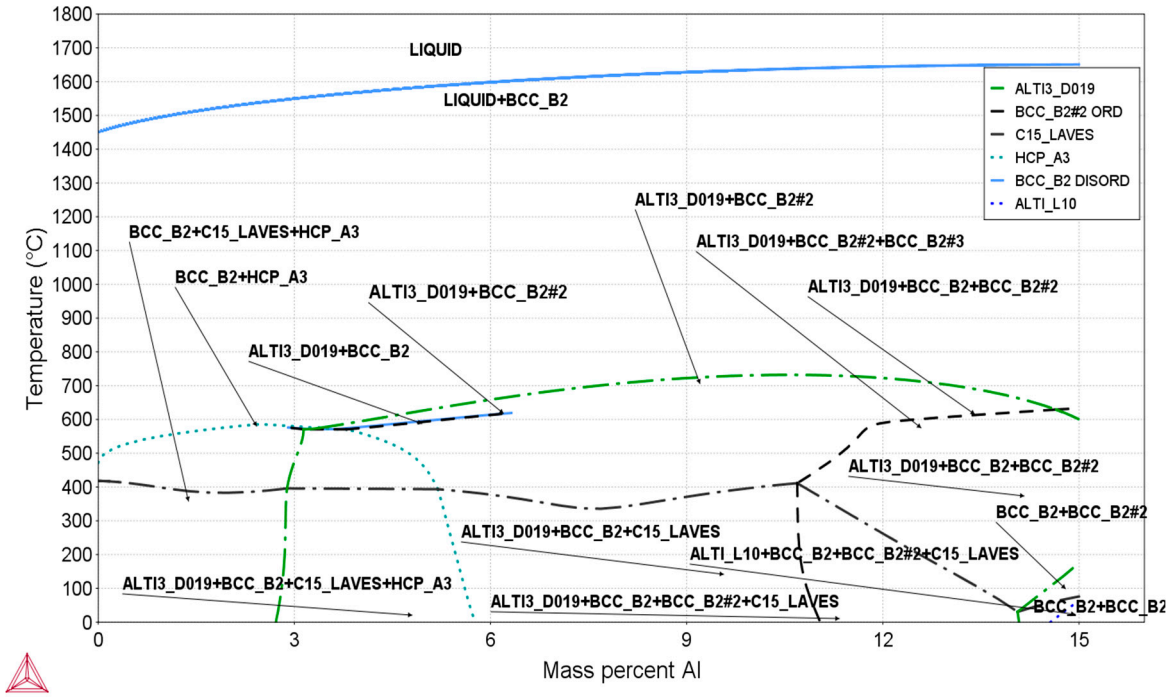

Figure 1. Phase diagram for one of the alloys from the Ti–Cr–Al–V system.

A matrix was created where 102 rows represent 102 Pareto-optimized candidate alloys taken from a previous work performed by Dulikravich et.al. [12]. The 57 columns are for 1 temperature, 4 alloying elements, 10 equilibrium phases (thus, 4 × 10 = 40 concentrations of alloying elements in the 10 equilibrium phases), and 2 properties (Young's modulus and density of the alloy). A number of the columns had many empty cells as not all of the equilibrium phases are stable for each candidate alloy. All of these columns are interrelated. Thus, we chose Self-organizing Maps (SOM) algorithm [20] in our work as it is known for capturing the topology of the multidimensional data sets.

The SOM algorithm is a classification technique that is based upon an unsupervised artificial neural network, popularly known as self-organizing feature maps (SOM) [17–22], which was popularized by Teuvo Kohonen in the 1980s. SOM implements a term competitive learning along with a neighborhood function to preserve the topological properties of the dataset [21]. This makes SOM a perfect tool to visualize high-dimensional datasets in lower dimensions—usually two to three—while preserving the topology for determining various correlations within the dataset [18]. SOMs can be considered as a nonlinear generalization of principal component analysis (PCA), an unsupervised machine learning method [20,22]. Recent studies demonstrated the advantage of using SOM over PCA [10,14].

Most importantly, SOMs have been successfully used for feature extraction of scarce datasets (sample size of about 40), whereas conventional neural networks require very large training datasets. In this work, we used SOM module in a commercial optimization package modeFRONTIER [16], which utilizes the following steps.

1. Scaling: Logistic scaling was used to minimize error.
2. Learning cycle: For our dataset, we used Batch SOM, where the learning cycle is updated after all the input samples are presented to the network (batch learning)
3. Set up training parameters: In the following text, key setting parameters are introduced, that were adjusted during the analysis.

    a. X-dimension and Y-dimension: It is an integer positive value and it represents the dimension of a component of the Kohonen map. The default value set by the toolbox was at 7 for X and 7 for Y.
    b. Map units: This is an integer positive parameter and it represents the dimension of the Kohonen map. The default value of 49 was set in this work so that the ratio between X-dimension and Y-dimension is equal to the ratio between the first two principal eigenvalues of the dataset matrix. Software suggests a default value based on the size of the dataset. From our experience, increasing this value usually improves accuracy, although it will take more time to develop the model.
    c. Initialization type: We used linear initialization where the initial map is obtained by using a linear combination of Kohonen map dimension and the two principal eigenvalues of the dataset.
    d. Random seed: This is an integer number, usually used for sequence repeatability. That is, if two SOMs are generated with the same seed, they will return identical maps. For a more random distribution, seed value can be set to 0. In this case, the map is automatically seeded with a value that is based on the current time on the computer which will rarely be same, and hence there is less chance of sequence repetition.

Development of the model is performed in two stages, initial rough phase and fine tuning phase. These radii are defined for these two stages of development of model. Therefore, there exist a few additional parameters, namely, initial rough radius, final rough radius, rough phase radius, initial fine tuning radius, final fine tuning radius, and fine tuning phase length. Rough phase and fine tuning are two stages during the development of the model, for which the radius is defined. All of these parameters have an integer positive value which needs to be fine-tuned during the analysis so as to minimize the topological error [16]. Topological error is a measure that represents the SOM's ability to show how well the SOM network reflects the relative position of sample data. As mentioned, adjacent SOM-units represents neighbor data in the input space. In the current work, topological error was zero.

Another error metric used for this work is quantization error, which was estimated at about 0.1. Quantization error is a measure of SOM's ability to learn from the data distribution. SOM is known for preserving the topology of the data set. In this work, very low topology error was observed for logistic scaling. When scaled by other approaches, this error was a nonzero number.

Our purpose of using SOM maps can be summarized as follows:

- Find correlations between various variables (alloying elements), volume fractions of equilibrium phases, concentrations of alloying elements in the equilibrium phases, and temperatures and properties that can be supported from the literature.
- Classify the dataset in various clusters and identify the units/clusters with candidate alloys having a set of superior properties. In our case, we marked the hexagonal units in the SOM maps with alloys that were part of the Pareto front of the best trade-off solutions when simultaneously maximizing Young's modulus and minimizing the density of the alloys [12].

- This method predicts the range of chemical compositions, temperatures, volume fraction of equilibrium phases, and concentrations of elements in equilibrium phases of alloys for superior properties.

This approach can be used as an additional screening tool for selecting a very small set of alloys to be manufactured in the next alloy design cycle.

3. Results

Our work in progress presented in this paper can be divided into three stages:

1. Stage 1: Determine the composition regime that we want to focus on for designing new titanium alloys for improved performance. The current work is the summary of stage 1 based on the equilibrium calculations performed under the framework of the CALPHAD approach. From this work, we have been able to determine the composition range that we will work on, the effect of temperature on the equilibrium phases for these compositions and associated macroscopic properties. We did not include a table for best alloys as, we have used 102 candidate alloys from our previous work, where we have tabulated the best performing alloy for each temperature.
2. Stage 2: In this stage, we will use the information from the Stage 1 and make an attempt to design and perform heat treatment simulations under the framework of CALPHAD approach. Our group has expertise in performing heat treatment simulations in Thermo-Calc Software [23–25]. One of the challenges in performing heat treatment simulations in any CALPHAD-based tools is the estimation of interfacial energy between the matrix phase and the precipitate phase. Interfacial energy is an important parameter that plays a key role in determining several aspects of heat treatment such as critical radius, activation energy, and nucleation rate in the early stages of the heat treatment, and coarsening rates that determine the final size of grains after annealing [25,26]. Several research groups have reported that CALPHAD-based tools overestimate the interfacial energy and, thus, it needs to be modeled carefully [25,26]. We have also published one paper [25] on this topic where we have demonstrated ways to address the discrepancy in interfacial energy, calculated through CALPHAD-based tools and the interfacial energy that will be helpful in properly simulating the experimental findings. In our recent work, we performed isothermal annealing in Thermo-Calc Software for simulating nucleation and growth of copper clusters in soft magnetic FINEMET alloys and verified our findings with atom Probe Tomography results. We noticed that for a small change in interfacial energy value from 0.54 to 0.64 J/m^2, mean radius increases from 2.5 nm to 20 nm for copper clusters in soft magnetic FINEMET alloys. To further increase in interfacial energy to 0.7, 0.75, and 0.8 J/m^2, mean radius becomes stagnant, but it is ~45 nm [26].
3. Stage 3: Once we optimize interfacial energy as a function of composition of the alloy and annealing temperature, we can proceed further towards performing experiments.

Figure 2 shows the SOM maps obtained from the above analysis for desired properties of interest (Young's modulus and density), temperature, and desired phases responsible for superior properties in (α + β) system, HCP_A3 (α), BCC_B2 (β_1), and BCC_B2#2 (β_2). In these figures, we have highlighted the hexagon units that contain alloys that were part of the Pareto front. There were 102 candidate alloys analyzed, and all the alloys were accommodated in 49 hexagonal units (0–48) of the SOM map. Within each hexagon, we can observe a square. Size of square determines the number of candidate alloys that were part of that hexagon unit. In some units, there is just a point. This means that no candidate alloys were part of this unit.

In the original dataset [12] of 104 Pareto-optimized Ti–Al–Cr–V candidate alloys, there were four candidate alloys with different compositions for temperatures of 30, 200, 400, 600, 800, and 1000 °C, while there were 20 candidate alloys with different compositions for each of the high temperatures (1200, 1300, 1400, and 1500 °C). Thus, there were 24 candidate alloys for temperatures below 1000 °C,

and 80 candidate alloys for temperatures above 1000 °C. Two candidate alloys were removed from the original dataset [12] as it was difficult to find equilibrium, thus, resulting in the final set of 102 Pareto-optimized candidate alloys that were then analyzed using SOM. Based on temperature, there were lower number of alloys below 1000 °C. As a result, candidate alloys for which calculations were performed below 600 °C became part of the hexagonal unit 0 in the SOM temperature map.

In order to study SOM maps in Figure 2, one must focus on the temperature range and then the associated property. It can be observed that for hexagonal unit 0, both Young's modulus and density are high. If one wants to study the properties at intermediate temperatures, they can focus on hexagonal unit 48, which again contains candidates with high Young's modulus and density. Similarly, if one wants to study alloys at high temperature, they must focus on hexagonal units 20 and 27, which contain candidates with high Young's modulus and near average density. Thus, from these SOM figures, an experimentalist can identify a set of candidate alloys at the desired temperature of application and then study their associated properties.

Thereafter, the reader can study the stable phases associated with those units. At high temperature (hexagonal units 20 and 27), one can observe that BCC_B2 (β_1) phase is stable. From the literature, it is known that α-phase is stable up to 885 °C and after that β-phase is stable up to melting point. However, in these SOM maps it can be observed that HCP_A3 (α) phase is present in some amounts at temperatures well above 885 °C. This is an interesting observation. Thus, an experimentalist must study the compositions for which HCP_A3 (α) phases are present in large amounts above 885 °C and check for stability of titanium aluminides and Laves phases for these compositions as these are present in titanium alloys with high aluminum content.

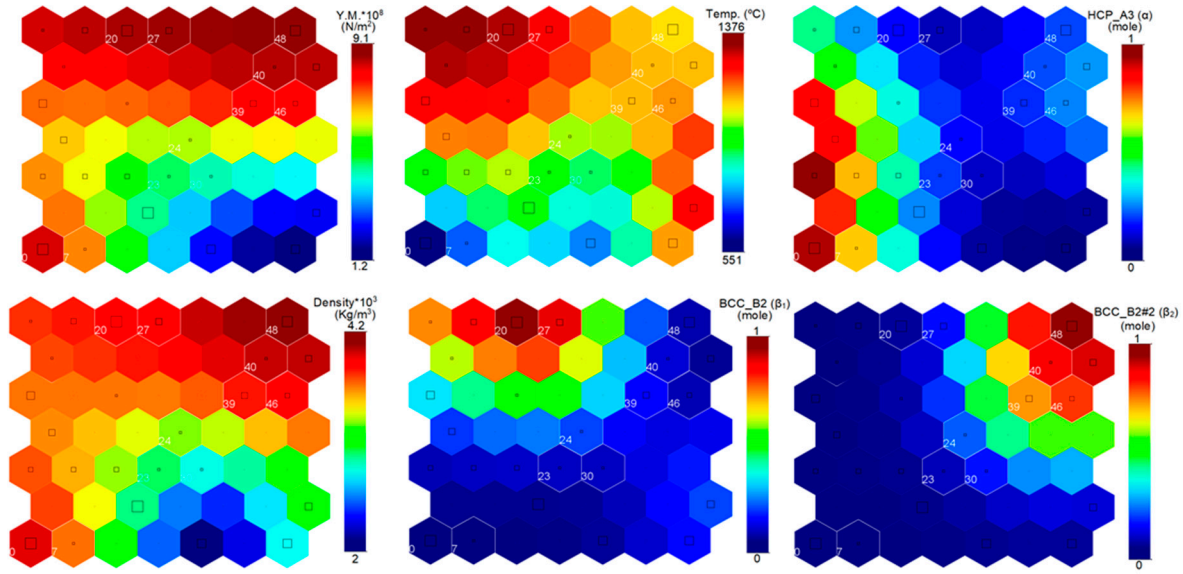

Figure 2. Correlation between desired phases, temperature, and properties.

Since the α-phase is responsible for superior properties at high temperature, this can be helpful in designing alloys for applications where a small amount of HCP_A3 (α) phase will be helpful. Up to 600 °C (unit 0), HCP_A3 (α) phase is stable as mentioned in the literature. For intermediate temperatures (unit 48), BCC_B2#2 (β_2) phase is stable. Thus, now we can proceed further to study the distribution of alloying elements in the SOM space.

As mentioned in the previous section, we will focus on α and β-phases only, as we are dealing with a (α + β) system. Hence, we will only briefly discuss undesirable phases, such as titanium aluminide and Laves phases shown in Figure 3, where one of the key findings is the appearance of liquid phase at intermediate to high temperatures. An experimentalist must avoid the alloy compositions which can have liquid phase at temperature of application. Another observation is that these titanium

aluminide phases are present in large number of candidate alloys that were not part of the original Pareto optimized set. Hexagonal units 7, 23, 24, and 30 in the SOM map shown in Figure 4 contain one candidate alloy each. The rest of the hexagonal units do not contain candidate alloys that were part of the original Pareto-optimized set of alloys where the amount of these titanium aluminide phases was stable in comparatively large amounts. This shows the efficacy of application of multiobjective design optimization combined with the SOM analysis.

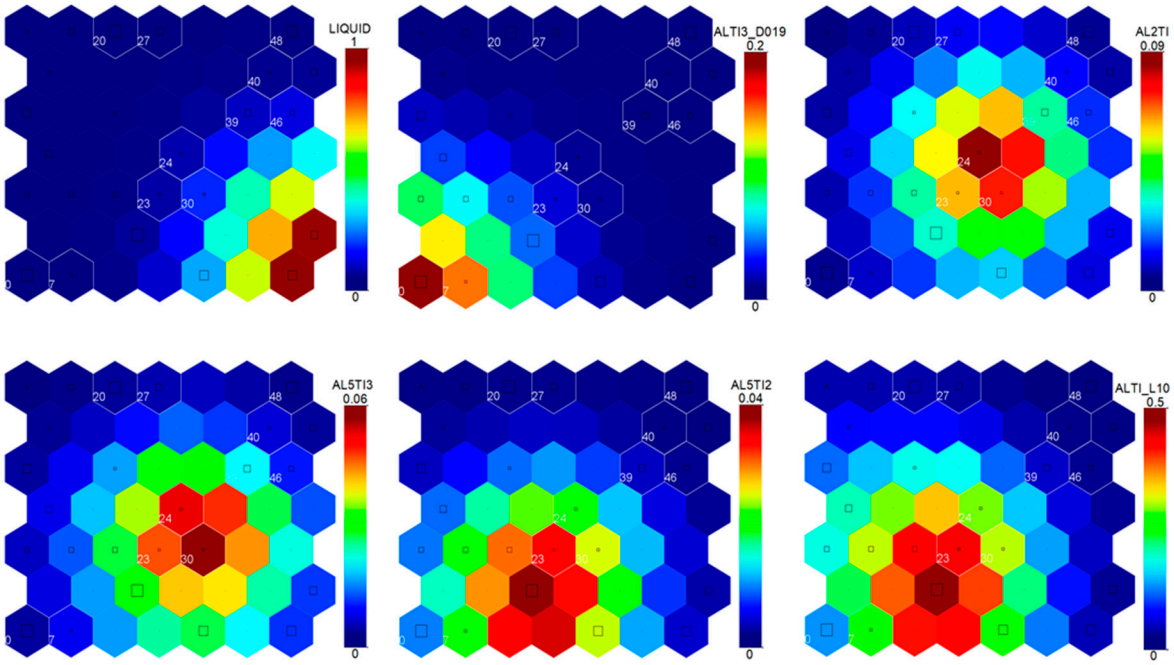

Figure 3. Phases that are not desired in the present system.

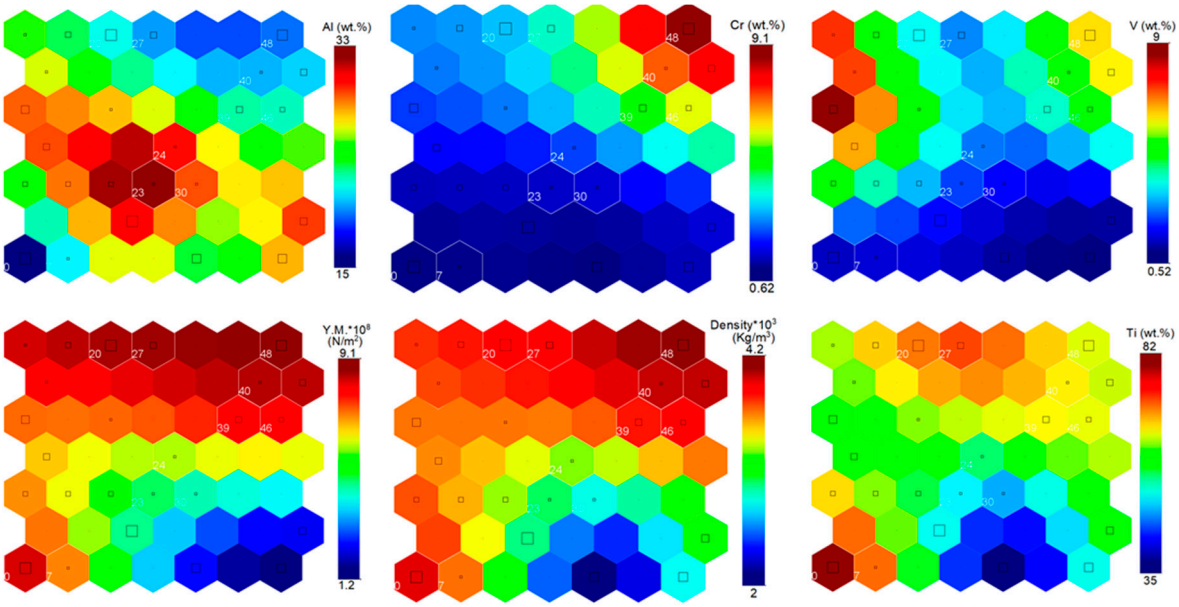

Figure 4. Correlation between alloying elements and desired properties.

Figure 4 shows the distribution of alloying elements, temperature and Young's modulus and density in the SOM space. From this important figure, the alloy designers can get an understanding regarding the composition regime/bounds that they must operate within to expect desired properties

of alloys at desired temperature. Additionally, they can compare it with Figures 2 and 3 and look at the desired phase they want in their system as well as the phases that they want to avoid.

In phase stability calculations, it was observed that for several candidate alloys the volume fraction of the desired phase was comparable, but the properties of alloys were different. Consequently, composition of phase was calculated and used in the SOM analysis. Another reason for this type of analysis was that there exist traces of HCP_A3 (α) at high temperatures and traces of BCC_B2 (β_1) at low temperatures. Hence, this analysis will be helpful for the readers to understand the reason for existence of HCP_A3 (α) at high temperatures and traces of BCC_B2 (β_1) at low temperatures, so that they can design the alloy compositions for desired temperature of application. Additionally, they can check if undesirable titanium aluminides are stable for these compositions.

Figure 5 shows the distribution of concentrations of alloying elements in HCP_A3 (α) phase where temperature was included for comparison. Here, it can be observed that in hexagonal unit 0 (average temperature: ~551 °C), candidate alloys are entirely HCP_A3 (α) and it is in accordance with the information reported in the literature [1]. There exists some trace amount of HCP_A3 (α) at higher temperatures in the non-Pareto candidate alloys around hexagonal unit 48. This is because in [4], a Pareto set was defined from a large number of virtually created alloys from response surfaces for each temperature. Thus, the rest of the alloys virtually generated in reference [12] were part of the non-Pareto set. Around unit 48, there is a moderate amount of aluminum, low vanadium, and chromium is comparatively high, but to a maximum of 1 g/mole, which is significantly low. Chromium is a β-stabilizer; thus, another reason for comparatively high chromium in unit 48 is that in this unit the BCC_B2#2 (β_2) phase is the stable phase. Figure 4 shows that hexagonal units around unit 48 contain the highest amount of chromium. Around hexagonal unit 20 (high-temperature), again, there are some trace amounts of HCP_A3 (α). Figure 5 shows that around hexagonal unit 20, the units contain low aluminum and negligible amount of chromium and vanadium (β-stabilizers). Also, it can be observed (Figure 4) that the unit adjacent to hexagonal unit 20 contains average aluminum, low chromium and average vanadium concentrations. Thus, Figures 4 and 5 can provide better understanding of the stability of β-phase at lower temperatures and appearance of trace amounts of α-phase at higher temperatures.

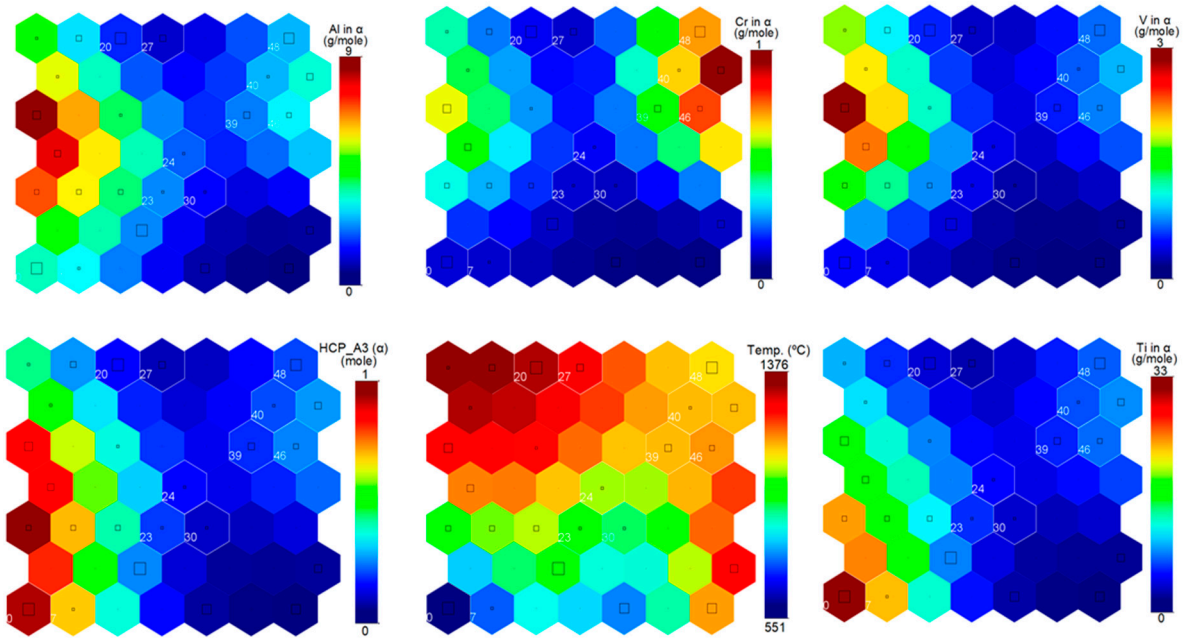

Figure 5. Distribution of alloying elements in the HCP_A3 phase.

Figure 6 shows the distribution of alloying elements in BCC_B2 (β_1) phase. In units on the right hand side of unit 27 temperature increases, while Young's modulus and density decrease (Figure 4), and aluminum content of β_1 phase increases. From Figure 4, it can also be observed that in units on the right hand side of unit 27 aluminum content of the alloys increases. Thus, one can conclude that increase in aluminum (an α-stabilizer) at elevated temperatures leads to an increase in aluminum content in the BCC_B2 (β_1) phase, which leads to a decrease in Young's modulus and density.

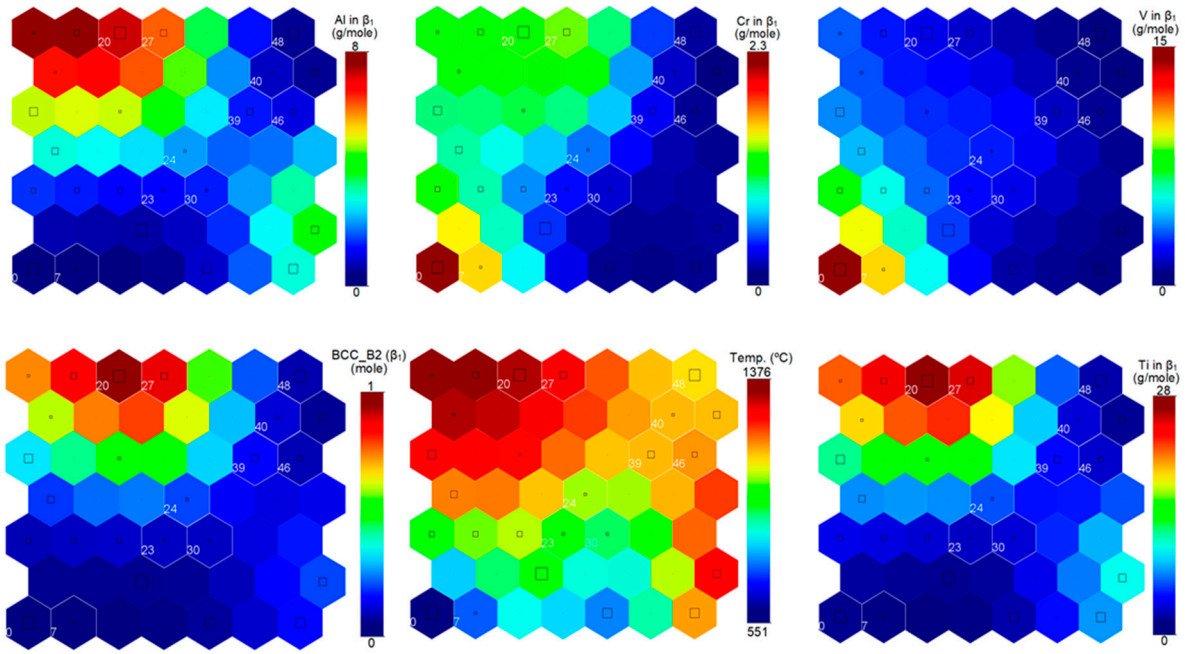

Figure 6. Distribution of alloying elements in BCC_B2 phase.

It can also be observed that in unit 0, for the composition of the BCC_B2 (β_1) phase, that there are high amounts of chromium and vanadium. This is expected [1] as hexagonal unit 0 is for temperatures below 600 °C. From literature [1], it is known that α to β transformations occur at around 785 °C. Thus, for even a trace amount of β-phase to appear at temperatures lower than 600 °C, composition of β-phase must be such that high amount of β-stabilizer elements is present. SOM maps are able to capture this complex trend. Hence, SOM analysis is able to draw correlations between the composition of alloy, stability of BCC_B2 (β_1) phase, composition of BCC_B2 (β_1) phase, temperature, and desired property.

Figure 7 shows the concentrations of alloying elements in BCC_B2#2 (β_2) phase. Hexagonal unit 48 contains candidate alloys with the highest amount of BCC_B2#2 (β_2). Temperature in this region is in the average range, while Young's modulus and density are the highest for this unit (Figure 4). From Figure 7, it can be observed that unit 48 contains the highest amount of chromium and vanadium (β-stabilizers) in BCC_B2#2 (β_2) phase and their contents decrease in the adjacent units.

Unit 48 also contains alloys with the highest Young's modulus and density and they decrease in the adjacent units. Even in Figure 4, hexagonal unit 48 contains alloys with highest amount of chromium, which decreases in the adjacent units, while it contains low amounts of aluminum, which increases in the adjacent units. Thus, a correlation can be drawn between the alloy composition (chromium content), stability of BCC_B2#2 (β_2) phase, phase composition (maximum chromium and vanadium in BCC_B2#2 (β_2) phase) and Young's modulus and density (highest) at an average temperature in unit 48. Additionally, the decrease of Young's modulus and decrease in density can be observed with change in alloy composition and phase composition in the adjacent units.

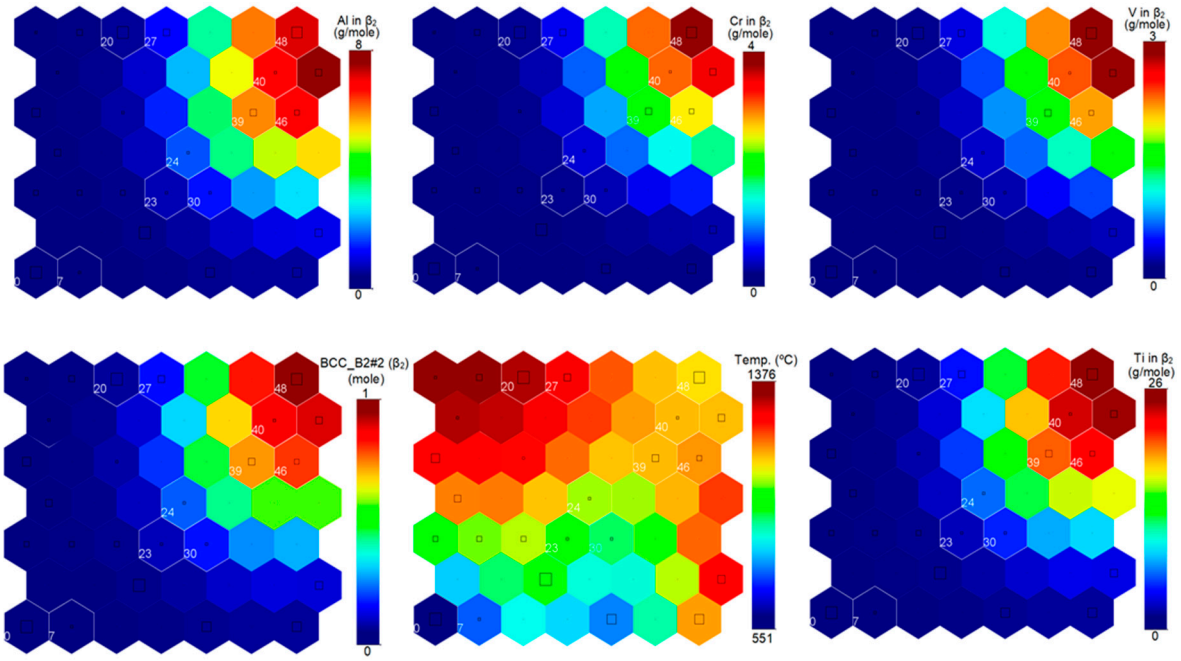

Figure 7. Distribution of alloying elements in the BCC_B2#2 phase.

4. Discussion

In this work, a novel attempt was made to use SOM analysis on already Pareto-optimized chemical compositions of a set of alloys to computationally correlate chemistry, stable phases, phase compositions, and targeted macroscopic properties of titanium alloys that will be helpful in the cost-effective computational design of optimized Ti–Al–Cr–V alloys at elevated temperatures. There is scope for future work, as we observed that the alloys for temperatures below 600 °C were clubbed in a single hexagonal unit 0 since only a limited amount of data was available for low temperature alloys. In the future, the entire range of temperatures from 30 to 1500 °C should be used for detailed study of the phase stability and transformations in this class of alloys.

Key findings from this work can be listed as follows.

- For high temperature (~1358 °C) the reader should analyze unit # 20. This unit contains alloys with high Young's modulus (~89600 N/m^2) and slightly above average density (~3920 kg/m^3). The stable phase for this unit is BCC_B2 (β_1). Average composition of alloys included in this unit is Al ~21.33 wt. %, Cr ~3.0 wt. %, V ~3.31 wt. %, and Ti ~71.68 wt. %.
- For average temperature (~1122 °C) the reader should analyze unit # 48. This unit contains alloys with high Young's modulus (~91000 N/m^2) and high density (~4170 kg/m^3). The stable phase for this unit is BCC_B2#2 (β_2). Average composition of alloys included in this unit is Al ~18.77 wt. %, Cr~9.06 wt. %, V ~6.23 wt. %, and Ti ~65.33 wt. %.
- For low temperature (~551 °C) the reader should analyze unit # 0. This unit contains alloys with high Young's modulus (~86800 N/m^2) and higher density (~4040 kg/m^3). The stable phase for this unit is HCP_A3 (α). Average composition of alloys included in this unit is Al ~14.93 wt. %, Cr ~0.64 wt. %, V ~1.00 wt. % and Ti ~81.74 wt. %.

It should be pointed out that this design methodology is applicable to other metallic alloy systems.

5. Conclusions

A computational methodology was presented to determine correlations between the chemical concentration of alloying elements, stability of desired phases over a range of temperatures, and their effect on multiple macroscopic properties of alloys. Additionally, the efficacy of using SOM maps in determining these correlations was demonstrated including an attempt to elucidate the deterioration of properties for candidate alloys having the same amount of desired phases by correlating them with the compositions of the desired phase. This study will be helpful to alloy designers in understanding the Ti–Al–Cr–V system and designing alloys that are expected to perform as per expectations at desired temperature of application. SOM maps were also able to capture the trends shown in a large dataset with many missing data as distribution of desired phases and the phase compositions appears in the same region on the SOM maps, even though SOM algorithm has no a priori information about the complex phase stability interrelations in multicomponent alloys. One of the drawbacks of the SOM algorithm is that the prediction accuracy is often not very high as the values are averaged over each hexagonal unit that can contain a maximum of six candidate alloys at its six vertices, while a few candidate alloys at the vertices can be part of more than one unit. This way, a candidate alloy can contribute to the average values of concentrations of alloying elements, volume fractions of phases, concentrations of alloying elements in the phases, and macroscopic properties over a unit for more than one unit. However, the SOM algorithm is able to capture the complete trend shown in the dataset.

Author Contributions: Conceptualization, R.J. and G.S.D.; Data curation, R.J.; Formal analysis, R.J. and G.S.D.; Investigation, R.J. and G.S.D.; Methodology, R.J.; Project administration, G.S.D.; Resources, R.J. and G.S.D.; Software, R.J.; Supervision, G.S.D.; Validation, R.J.; Visualization, R.J.; Writing—original draft, R.J.; Writing—review & editing, R.J. and G.S.D.

Funding: This research received partial funding from National Aeronautics and Space Administration (NASA) University Leadership Initiative (ULI) program administered by Texas A&M University (TAMU) under federal award number NNX17AJ96A, titled "Adaptive Aerostructures for Revolutionary Supersonic Transportation".

Acknowledgments: The lead author is thankful to John Volakis, Dean, College of Engineering and Computing, Florida International University for partially financially supporting his postdoctoral experience. Authors would also like to express their sincere gratitude to Carlo Poloni, founder and president of ESTECO, for providing modeFRONTIER optimization software for this project.

Conflicts of Interest: The authors declare no conflict of interest. The funders had no role in the design of the study; in the collection, analyses, or interpretation of data; in the writing of the manuscript, or in the decision to publish the results.

References

1. Polmear, I.; John, D.; Nie, J.-F.; Qian, M. (Eds.) Chapter 7—Titanium Alloys. In *Light Alloys*, 5th ed.; Butterworth-Heinemann, Elsevier: Oxford, UK, 2017; pp. 369–460.
2. Polmear, I.; John, D.; Nie, J.-F.; Qian, M. (Eds.) Chapter 8—Novel Materials and Processing Methods. In *Light Alloys*, 5th ed.; Butterworth-Heinemann, Elsevier: Oxford, UK, 2017; pp. 461–514.
3. Gupta, R.K.; Pant, B. *Chapter 4—Titanium Aluminides. Intermetallic Matrix Composites*; Mitra, R., Ed.; Woodhead Publishing, Elsevier: Duxford, UK, 2018; pp. 71–93.
4. Boyer, R.R. An overview on the use of titanium in the aerospace industry. *Mater. Sci. Eng.* **1996**, *213*, 103–114. [CrossRef]
5. Wu, X.-H. Review of alloy and process development of TiAl alloys. *Intermetallics* **2006**, *14*, 1114–1122. [CrossRef]

6. Dulikravich, G.S.; Egorov, I.N.; Sikka, V.K.; Muralidharan, G. Semi-stochastic optimization of chemical composition of high-temperature austenitic steels for desired mechanical properties. In Proceedings of the 2003 TMS Annual Meeting Yazawa International Symposium: Processing and Technologies, San Diego, CA, USA, 2–6 March 2003; Kongoli, F., Itakagi, K., Yamaguchi, C., Sohn, H.-Y., Eds.; TMS Publication: San Diego, CA, USA, 2003; pp. 801–814.
7. Egorov-Yegorov, I.N.; Dulikravich, G.S. Chemical composition design of superalloys for maximum stress, temperature and time-to-rupture using self-adapting response surface optimization. *Mater. Manuf. Process.* **2005**, *20*, 569–590. [CrossRef]
8. Dulikravich, G.S.; Egorov, I.N.; Colaco, M.J. Optimizing chemistry of bulk metallic glasses for improved thermal stability. *Model. Simul. Mater. Sci. Eng.* **2008**, *16*, 075010. [CrossRef]
9. Bhargava, S.; Dulikravich, G.S.; Murty, G.; Agarwal, A.; Colaco, M.J. Stress corrosion cracking resistant aluminum alloys: Optimizing concentrations of alloying elements and tempering. *Mater. Manuf. Process.* **2011**, *26*, 363–374. [CrossRef]
10. Jha, R.; Dulikravich, G.S.; Chakraborti, N.; Fan, M.; Schwartz, J.; Koch, C.C.; Colaco, M.J.; Poloni, C.; Egorov, I.N. Algorithms for design optimization of chemistry of hard magnetic alloys using experimental data. *J. Alloy. Compd.* **2016**, *682*, 454–467. [CrossRef]
11. Dulikravich, G.S.; Egorov, I.N. Inverse Design of Alloys' Chemistry for Specified Thermo-Mechanical Properties by Using Multi-Objective Optimization. In *Computational Methods for Applied Inverse Problems*; Wang, Y.F., Yagola, A.G., Yang, C.C., Eds.; Inverse and Ill-Posed Problems Series 56; Walter De Gruyter and Higher Education Press: Beijing, China, 2012; Chapter 8, pp. 197–219, ISBN 978-3-11-025905-6.
12. Dulikravich, G.S.; Kumar, A.; Egorov, I.N. Titanium based alloy chemistry optimization for maximum strength, minimum weight and minimum cost using JMatPro and IOSO software. In Proceedings of the TMS Annual Meeting, Materials Informatics: Enabling Integration of Modeling and Experiments in Materials Science, New Orleans, LA, USA, 9–13 March 2008.
13. JMatPro. Available online: https://www.sentesoftware.co.uk/jmatpro.aspx (accessed on 20 February 2019).
14. Egorov, I.N. Indirect optimization method on the basis of self-organization. In Proceedings of the Optimization Techniques and Applications (ICOTA'98), Perth, Australia, 1–3 July 1998; Volume 2, pp. 683–691.
15. Thermo-Calc Software. Available online: https://www.thermocalc.com/solutions/by-material/titanium-based-alloys/ (accessed on 20 February 2019).
16. ESTECO: modeFRONTIER. Available online: http://www.esteco.com/modefrontier (accessed on 20 February 2019).
17. Wikipedia. Self-Organizing Map. Available online: https://en.wikipedia.org/wiki/Self-organizing_map (accessed on 20 February 2019).
18. Liu, Y.; Weisberg, R.H.; Mooers, C.N.K. Performance evaluation of the self-organizing map for feature extraction. *J. Geophy. Res.* **2006**, *111*, C05018. [CrossRef]
19. Yin, H. Learning Nonlinear principal manifolds by self-organising maps. In *Principal Manifolds for Data Visualization and Dimension Reduction*; Gorban, A.N., Kégl, B., Wunsch, D.C., Zinovyev, A.Y., Eds.; Lecture Notes in Computational Science and Engineering; Springer: Berlin, Germany, 2008; Volume 58, pp. 68–95.
20. Jha, R.; Dulikravich, G.S.; Chakraborti, N.; Fan, M.; Schwartz, J.; Koch, C.C.; Colaco, M.J.; Poloni, C.; Egorov, I.N. Self-organizing maps for pattern recognition in design of alloys. *Mater. Manuf. Process.* **2017**, *10*, 1067–1074. [CrossRef]
21. Pena, M.; Barbakh, W.; Fyfe, C. Topology-preserving mappings for data visualization. In *Principal Manifolds for Data Visualization and Dimension Reduction*; Gorban, A.N., Kégl, B., Wunsch, D.C., Zinovyev, A.Y., Eds.; Lecture Notes in Computational Science and Engineering; Springer: Berlin, Germany, 2008; Volume 58, pp. 131–150.
22. Krasznai, E.Á.; Boda, P.; Csercsa, A.; Ficsór, M.; Várbíró, G. Use of self-organizing maps in modelling the distribution patterns of gammarids (Crustacea: Amphipoda). *Ecol. Inform.* **2016**, *31*, 39–48. [CrossRef]
23. Jha, R.; Diercks, D.R.; Stebner, A.P.; Ciobanu, C.V. Metastable phase diagram and precipitation kinetics of magnetic nanocrystals in FINEMET alloys. *Condens. Matter* **2017**, arXiv:1709.08306.
24. Jha, R.; Chakraborti, N.; Diercks, D.R.; Stebner, A.P.; Ciobanu, C.V. Combined machine learning and CALPHAD approach for discovering processing-structure relationships in soft magnetic alloys. *Comp. Mater. Sci.* **2018**, *150*, 202–211. [CrossRef]

25. Jha, R.; Diercks, D.R.; Chakraborti, N.; Stebner, A.P.; Ciobanu, C.V. Interfacial energy of copper clusters in Fe-Si-B-Nb-Cu alloys. *Scripta. Mater.* **2019**, *162*, 331–334. [CrossRef]
26. Meher, S.; Carroll, M.C.; Pollock, T.M.; Carroll, L.J. Designing nickel base alloys for microstructural stability through low γ-γ′ interfacial energy and lattice misfit. *Mater. Des.* **2018**, *140*, 249–256. [CrossRef]